IEEE Access
Multidisciplinary | Rapid Review | Open Access Journal

Received February 14, 2020, accepted March 10, 2020, date of publication March 30, 2020, date of current version April 27, 2020.

Digital Object Identifier 10.1109/ACCESS.2020.2983919

Space-Time Modeling of Rainfall Rate for Satellite Networks

GUANGGUANG YANG[1], DAVID L. NDZI[2], ABDUL-HADI AL-HASSANI[3], MISHA FILIP[4], AND DAVID PAUL[5]

[1]Department of Electronic Engineering, Foshan University, Foshan 528225, China
[2]School of Computing Engineering and Physical Sciences, University of the West of Scotland, Paisley PA1 2BE, U.K.
[3]Iraq University College, Basrah 61004, Iraq
[4]Faculty of Technology, University of Portsmouth, Portsmouth PO1 3AH, U.K.
[5]Cordovan Branding Limited, Teddington TW11 8HG, U.K.

Corresponding author: David L. Ndzi (david.ndzi@uws.ac.uk)

ABSTRACT A new comprehensive space-time model for the characterization of point rainfall rate is presented. A detailed assessment of four key rain characteristics (probability of rain/no rain condition, first and second order lognormal statistics and, space and time correlation functions) with consideration of the impact of varying spatial-temporal integration lengths are discussed. A set of empirical equations have been developed and the results show that they provide estimates of probability of rain/no rain with root mean square errors of less than 1.3 in space and 0.04 in time. They provide good estimates of the parameters at any space-time scales, particularly at higher resolutions that are of great importance to the design and planning of networks operating at frequencies above 10 GHz. In particular, the authors have created databases of rain characteristic parameters spanning North West Europe from which rain rate at any location of interest at different space-time scales can be conveniently obtained. These have been validated by comparing the rain rate exceedance distribution, $R_{0.01}$, from the model estimates at different space-time scales across the British Isles with values calculated from measured data. It has been found that the proposed model gives highly accurate estimates of $R_{0.01}$ for the continental area with error percentages (E) generally less than 2.5 but the error percentage increases at the edges of the radar scans and in the oceanic area due to low data availability.

INDEX TERMS Rainfall rate, rain characteristics, radio-wave propagation, space-time model, satellite.

I. INTRODUCTION

Wireless communication systems operating at frequencies greater than 10 GHz are significantly affected by rain attenuation of radio waves, which leads to poor network performance [1]–[3]. This is particularly true for millimeter wave communication links where the rainfall rate for 0.01% of the time is an important parameter [4]. Rain events are highly variable in both space and time and their characteristics are influenced by factors such as climate type, season and topography [5]. A quantitative understanding of the behavior of the spatial and temporal variability of rain is required to calculate the long-term rain-induced attenuation statistics, e.g. ITU-R P.618-12 [6].

The extremely variable nature of rain makes it challenging to estimate rain rates over large areas with high resolutions directly from measurements. Although this can potentially be achieved with a high density network of rain gauges, the cost of such a deployment is prohibitive and difficult to cover wide areas with suitable space resolutions (say L). Therefore the data that is available is often estimates at one point rather than an area covered by multiple points. Meteorological radar and satellite measurements compensate this drawback and can capture the fine-scale spatial variability of rainfall, but the time resolution (say T) is often poor. In addition, it is difficult to obtain accurate rainfall rate measurements over mountain and oceanic areas due to difficulties associated with obtaining accurate rain radar readings [7]. Such limitations have been addressed using rain models, for example in [9]–[11].

Rain modeling has evolved to ameliorate the limited resolutions of measurement apparatus to offer other resolutions, particularly at smaller scales L' and T', using approaches such as downscaling [12], [13], fractal theory (self-similarity) [14], [15], and interpolation [16], [17]. However, the drawback in most of the existing rain studies is that they tend to purely focus on predictions at either smaller space scales, so

The associate editor coordinating the review of this manuscript and approving it for publication was Hayder Al-Hraishawi.

evolution in time of spatial patterns of rain field is not considered, [18], [19], or shorter time scales without explicitly taking the spatial distribution of rain fields into account [20], [21]. However, rain exhibits high variability and irregularity in both space and time. High intensity rain events, especially those associated with strong convection, normally cover only a few kilometers and last for short periods. These cause severe outage in high frequency wireless networks. The 3D space-time point rain rate data at higher resolutions, which is often not available from commonly used apparatus, is of particular importance to describe these small-scale events and is required by networks planners and designers of physical layer fade mitigation techniques [22], [23]. A representative model of rain dynamics would be a combination of a two-dimensional model in space and a one dimensional model in time.

The lack of three-dimension (3D) space-time modeling of rain has long been a challenging issue and there are only a few studies that have been published in the past few decades. For example, taking advantage of the spatial disaggregation scheme, like in [24], Venugopal in [25] proposed a space-time downscaling model utilizing dynamic scaling property in rainfall to predict spatially evolving rainfall fields which preserve a prescribed space-time organization structure at finer scales. Another classic space-time rain model was proposed by Deidda *et al.* [26] based on the assumption that Taylor's hypothesis [27] can be applied. The space and time scales, therefore, can be connected and then mutually-converted using an advection velocity parameter so that the statistical properties of rain at smaller scales can be deduced from larger ones. Instead of focusing on rain rate only, alternative studies of rain characteristics have also attracted a lot of interest [28]–[31]. This is because in [32] Bell has demonstrated that a reasonable lognormal distribution of rain fields can be simulated provided systematic knowledge of the key rain characteristics are known. Therefore, in [33], the authors have proposed a new space-time interpolation approach that can interpolate the key rain characteristics to finer scales of the order of seconds, in time, and meters, in space, with high accuracy.

In particular, the authors proposed a statistical model in [34] based on the assessment of the impact of varying spatial and temporal integration lengths on key characteristics of point rainfall rate and their dependencies on the integration volumes. However, the proposed model is only valid for cases where either the spatial or temporal integration length is constant (C), whilst the other is changing, denoted as: $\{L, T = C\}$ or $\{L = C, T\}$. As an extension of the work in [34], this paper aims to fulfill two objectives: 1) assess the impact of varying $3D$ spatial-temporal integration lengths on rain; and 2) develop an appropriate model to estimate the rain characteristics at changing space-time scales, particularly at smaller ones. These objectives, when fulfilled, will enable the estimation of point rainfall rate at any given scale together with the prediction of rain-induced attenuation for wide area networks with multiple links of varying lengths.

The reminder of this paper is organized as follows; Section II describes the experimental data used in this study. Section III discusses the methodology for modeling the point rainfall rate and briefly describes how to generate rain fields using rain parameters. Section IV presents the experimental results and the proposed empirical equations for estimating rain characteristics at different space-time scales. We have also validated the results using real measurements from datasets with better resolution. Conclusions are drawn in Section V.

II. DATA DESCRIPTION

The experimental data used in this study is provided by the Centre for Environmental Data Analysis (CEDA), which holds a database of European rainfall rate estimate generated by NIMROD radar system. This covers several climatic zones. The NIMROD system concurrently receives the radar images from 15 C-band (5.3 cm wavelength) radars. The radar network performs a series of 15-minute azimuth scans at different elevations and converts the rainfall rate data onto a 5-km Cartesian grid [35], [36]. The composite European data is available from April 2002 as well as radar images from 1999. The processed radar and satellite data together with surface reports and Numerical Weather Prediction (NWP) fields are jointly used for precipitation rate analysis [37]. In this study, five years of radar data from 2010 to 2014 has been studied. The dataset used consists of more than 150,000 radar maps with each map covering 432,000 grid points.

CEDA also holds another dataset with better resolution over the British Isles. Radar networks within the UK have several scan radii with space resolution up to $1km$ at time intervals as short as $5mins$ (see [38]).

III. SPACE-TIME MODELING OF POINT RAIN RATE

The prediction of the dynamic rain attenuation statistics in slant paths is required in many applications relating to satellite communication. Matricciani in [39] has proposed a physical-mathematical model using a method known as ''synthetic storm technique'' for calculating the rain attenuation. The specific attenuation may be calculated from raindrop size distribution but an adequate approximation may be obtained from the rain rate. Rec. ITU-R P. 838-3 [40] provides a power-law model linking specific attenuation γ and rainfall rate $R(mm/h)$ as follows;

$$\gamma \cong \alpha R^{\beta} \tag{1}$$

where α and β are frequency dependent parameters.

Given that the average rainfall rate measured within a spatial area $A = L \times L$ at time interval T is expressed as:

$$R(L, T) = \frac{1}{T} \int_{\_T/2}^{T/2} dt \int_{\_L/2}^{L/2} \int_{\_L/2}^{L/2} r(\mathbf{x}, t) da \tag{2}$$

where $r(\mathbf{x}, t)$, here $\mathbf{x} = (x_1, x_2)$, denotes the point rainfall rate in mm/h at location $\mathbf{x}$ and time t. L and T are the spatial and temporal integration lengths of NIMROD radar map, respectively.

The synthesis of rain fields requires detailed understanding of four key characteristics of rain; the probability of rain occurrence, first order statistics and, space and time correlation function of rain [32]–[34]. It has been demonstrated that point rainfall rate at one location for any combination of spatial and temporal integration length is well modeled as a lognormal process with a mixed probability density function (PDF) [41]:

$$\Lambda_R(\mu,\sigma,P_0)=\begin{cases}1-P_0 & \text{no rain}\\ \dfrac{P_0}{\sqrt{2\pi}R\sigma}exp\left[-\left(\dfrac{lnR-\mu}{\sigma}\right)^2\right] & \text{for rain}\end{cases} \tag{3}$$

where P_0 denotes the probability of rain occurrence at a point when it is raining ($R > 0$), and $\{\mu,\sigma\}$ are the lognormal parameters required to describe the distribution of rainfall rate, where μ and σ are the mean and standard deviation of R, respectively. Previous study in [34] showed that the statistical parameters $\{P_0,\mu,\sigma\}$ depend on the location $\mathbf{x}$ and the integration volume. P_0 is equivalent to the long term probability of rain over a period $\mathcal{T}$ i.e $P_0 = \mathcal{T}_{rainy}/\mathcal{T}$. The general empirical equation that gives good estimates of P_0 throughout the whole range of integration length is:

$$P_0 = 100 - bexp\left(cx^e\right) \tag{4}$$

where b, c and e are model coefficients which can be determined for each location and x denotes either spatial integration length L, or temporal integration length T.

It has been shown in [32] that a zero mean, unit variance discrete Gaussian field, $g(\mathbf{x})$, can be modeled with a spatial covariance predetermined by the desired rain field covariance. Over long term periods i.e. many 2D maps $g_t(\mathbf{x})$, the Gaussian field can be transformed into a rain field $r(g_t(\mathbf{x}))$ using nonlinear transformation:

$$r\{g_t(\mathbf{x})\} = \begin{cases}0, & g_t(\mathbf{x}) < g_0\\ \exp\left(\sigma Q^{-1}\left(\dfrac{Q(g_t(\mathbf{x}))}{P_0}\right)+\mu\right), & \text{otherwise}\end{cases} \tag{5}$$

then a rain field with the PDF in Eq. (3) can be produced provided $g_0 = Q^{-1}(P_0)$ is the chosen threshold, here

$$P_0 = \int_{g_0}^{\infty}\frac{1}{\sqrt{2\pi}}\exp\left(-\frac{u^2}{2}\right)du \equiv Q(g_0) \tag{6}$$

It is worth highlighting that the above transformation links to the correlation coefficient ρ of the Gaussian rain field. The space correlation function, which is equal to the inverse Fourier transform of the normalized spectrum, is always used to assess the horizontal structure of rainfall field. Given that rain is wide sense stationary, the time correlation function strongly depends on the time difference between t_1 and t_2.

The correlation function of rainfall rate can be expressed as [42];

$$\rho_R = \frac{E\left\{R_iR_j\right\}-E\{R_i\}E\left\{R_j\right\}}{\sqrt{var(R_i)\,var\left(R_j\right)}} = \frac{cov\left(R_i,R_j\right)}{\varepsilon_i\varepsilon_j} = \Upsilon(\rho) \tag{7}$$

TABLE 1. Probability of rain occurrence (%) for increasing spatial-temporal integration lengths ranging from 5 *km* to 75 *km* and 15 *mins* to 120 *mins* at Portsmouth.

	$T(mins)$							
$L(km)$	15 *mins*	30 *mins*	45 *mins*	60 *mins*	75 *mins*	90 *mins*	105 *mins*	120 *mins*
5 *km*	18.67	22.86	25.90	28.51	30.55	32.64	34.33	36.07
10 *km*	23.43	28.62	32.28	35.01	37.44	40.04	41.12	43.24
15 *km*	28.64	33.74	37.55	40.32	42.88	44.91	46.74	48.59
20 *km*	32.59	37.93	41.59	44.69	47.14	49.37	51.40	53.14
25 *km*	35.25	40.58	46.15	48.21	51.49	54.67	56.73	59.23
35 *km*	42.49	48.33	52.25	55.42	57.91	60.11	61.97	63.07
40 *km*	47.86	53.40	55.19	58.11	61.86	63.22	64.01	66.15
45 *km*	48.81	55.64	59.46	62.24	64.66	66.64	69.18	70.62
50 *km*	51.87	56.17	60.18	63.97	65.59	67.17	70.21	71.45
55 *km*	56.51	62.15	65.80	68.48	70.73	72.21	73.51	75.30
65 *km*	60.98	65.52	68.51	70.64	72.30	74.23	75.77	76.45
75 *km*	63.88	69.06	72.41	74.45	76.29	78.79	79.68	80.93

where R_i and R_j are the point rainfall rates at either two locations or two times i and j, $cov()$ is the covariance and ε is the variance with $|\rho| \le 1$ and $cov\left(R_i,R_j\right) \le \varepsilon_i\varepsilon_j$.

The correlation of rainfall rate can be calculated from radar-derived rain rate and ρ can be obtained using functional inverse $\rho = \Upsilon^{-1}(\rho_R)$, see [41]. Taking the correlation coefficient into account, a logical extension of Eq. (3) is that the distribution of rain rate at two points on a horizontal plane at a particular time or two time periods at the same location is jointly lognormal with the joint PDF (see [3]):

$$\begin{aligned} &f(R_1,R_2,\rho)\\ &=\frac{1}{2\pi\sigma_1\sigma_2R_1R_2\sqrt{1-\rho^2}}\exp\left(-\frac{1}{2\left(1-\rho^2\right)}\right.\\ &\cdot\left(\left(\frac{lnR_1-\mu_1}{\sigma_1}\right)^2-\frac{(lnR_1-\mu_1)(lnR_2-\mu_2)}{\sigma_1\sigma_2}\right.\\ &\left.\left.+\left(\frac{lnR_2-\mu_2}{\sigma_2}\right)^2\right)\right) \end{aligned} \tag{8}$$

For simplicity, Eq. (8) can be denoted as

$$f(R_1,R_2,\rho) = \Psi_{R_1,R_2}(\mu_1,\sigma_1,\mu_2,\sigma_2) \tag{9}$$

where parameters $\{\mu_k,\sigma_k\}, k = 1,2$ describe the lognormal statistics of point rain rate at either two locations or two time periods of interest. The four parameters at varying integration lengths can be estimated from empirical distribution function of rainfall rate using the technique proposed in [43].

IV. INTEGRATION AND DOWNSCALING OF RAIN CHARACTERISTICS

A. PROBABILITY OF RAIN OCCURRENCE

To assess the impact of space-time averaging on rain intermittence, the theory presented in [34] and the mixed rain distribution in Eq. (3) can be used to obtain P_0 at different space-time scales. In this paper, P_0 at increasing spatial-temporal integration lengths ranging from $5km$ to $75km$ and $15mins$ to $120mins$ at all locations within the studied area have been analyzed. Taking Portsmouth as an example, the probability of rain occurrence at 96 space-time combinations have been calculated and listed in Table 1.

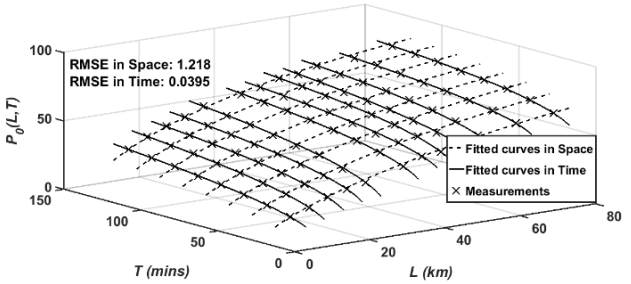

FIGURE 1. Plot of P_0 distribution for increasing spatial and temporal integration length at Portsmouth in the southern UK.

TABLE 2. Equation 11 fitted coefficients for a range of spatial integration lengths at Portsmouth.

T $(mins)$	b	c	e
15 $mins$	88.8065	−0.0219	0.8638
30 $mins$	84.8571	−0.0233	0.8755
45 $mins$	81.9313	−0.0239	0.8922
60 $mins$	79.3851	−0.0248	0.8952
75 $mins$	77.4635	−0.0256	0.9013
90 $mins$	75.5877	−0.0268	0.9063
105 $mins$	74.0168	−0.0277	0.9091
120 $mins$	72.2612	−0.0283	0.9104

TABLE 3. Equation 12 fitted coefficients for a range of temporal integration lengths at Portsmouth.

L (km)	b	c	e
5 km	90.7081	−0.0239	0.5608
10 km	91.3798	−0.0483	0.4792
15 km	87.9657	−0.0618	0.4503
20 km	83.8751	−0.0614	0.4688
25 km	82.8319	−0.0634	0.5011
35 km	73.0206	−0.0588	0.5175
40 km	65.7772	−0.0588	0.5074
45 km	71.0355	−0.0894	0.4796
50 km	58.6189	−0.0361	0.6269
55 km	58.6876	−0.0738	0.5175
65 km	52.7114	−0.0824	0.4781
75 km	50.5571	−0.0824	0.5193

Whilst it is challenging to derive a physical model for rain intermittence, modeling P_0 based on the calculated values is more expeditious. Eq. (4) can be used for downscaling P_0 to other space and time scales, particularly those smaller than radar estimates.

Table 2 and 3 list the fitted coefficient values of Eq. (4)for space domain and time domain, respectively. Using these coefficients together with values from Table 1, we can produce a 3D space-time plot of $\boldsymbol{P_0}$ distribution as shown in Fig. 1. For small space-time scales, it is realistic to assume that $\boldsymbol{P_0}\,(\boldsymbol{L}\to\boldsymbol{0},\boldsymbol{T}\to\boldsymbol{0})\ \to\boldsymbol{0}$ and for large scales, $\boldsymbol{P_0}\,(\boldsymbol{L}\to\infty,\boldsymbol{T}\to\infty)\to\boldsymbol{1}$.

It is therefore adequate to re-evaluate Eq. (4) to produce a space-time prediction formula for P_0 in 3D space-time scales:

$$P_0\,(L,T)=100-bexp\left(c_L L^{e_L}+c_T T^{e_T}\right) \qquad (10)$$

From UK NIMROD radar data at Portsmouth, the calculated $P_0\,(L=1km,T=5mins)\ =\ 12.56$, whilst the estimated $P_0\,(L=1km,T=5mins)$ from Eq. (10) is 12.18, giving a difference of 3%. This is deemed to be acceptable taking into account the varying space-time resolutions.

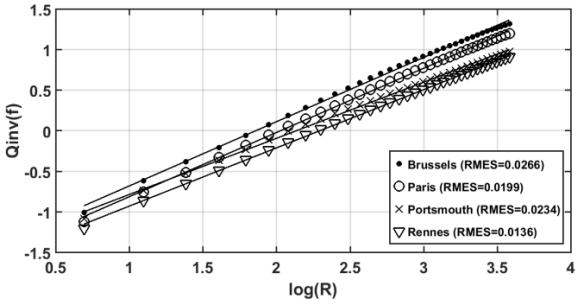

FIGURE 2. Test for log-Normality of rainfall rate distribution for each location with space resolution of 5*km* and time intervals of 15*mins*. The dots are values calculated from measured radar data and the straight lines (fitted curves) are transformed CCDF using the fitting method described in [43].

Therefore for Portsmouth, Eq. (10) can be expressed as.

$$\begin{aligned}&P_{\text{Portsmouth}}(L,T)\\&=100-92.12\\&\quad*\exp\left(-0.0215*L^{0.8211}-0.0125*T^{0.6383}\right)^{1}\end{aligned} \qquad (11)$$

Similar results can be produced for any location within the studied region of North West Europe.

B. STATISTICS OF RAIN

The statistics of rainfall rate over a grid area were computed to obtain the values for each central location. The area size $\mathcal{A}=400km\times400\,km$ was chosen as studies in [44] have shown that log-normal parameters $\{\mu,\sigma\}$ become stable and converge to virtually constant values for any combination of spatial and temporal integration lengths when $\mathcal{A}\ >\ 350\,km\ \times\ 350\,km$. Using the technique described in [43], the transformed complementary cumulative distribution function (CCDF) can be achieved together with estimates of the log-normal parameters $\{\mu,\sigma\}$.

Fig. 2 shows the test for log-Normality of rainfall rate distribution for four locations. The straight lines clearly shows that rain rate at each location is log-normally distributed. The log-Normality property of rain can be observed at other space-time combinations (for brevity other results are not presented in this paper). It has also been found that the log-normal parameters exhibit monotonous changes. To be specific, μ gradually decreases with increasing integration length while σ shows a completely opposite tendency. This paper presents some of the derived values of $\{\mu,\sigma\}$ at Portsmouth with increasing spatial integration lengths ranging from 5 km to 75 km and the temporal periods between 15 $mins$ and 120 $mins$ to show these tendencies, see Table 4.

Fig. 3, as an example, shows that the log-normal parameters, in both space and time, can be approximated by a second

[1]Note: The fitted coefficient values given in Eq. (11) are examples that estimate the smaller space-time scales values of interest. So the accuracy for large scales is relatively low. However, the values are adjustable to meet the requirements of users (i.e. other range of scales).

TABLE 4. Experimental value of log-normal distributions for increasing scale at Portsmouth.

	$T = 15\ mins$			$L = 5\ km$	
$L\ (km)$	μ	σ	$T\ (mins)$	μ	σ
5	-4.7793	1.8784	15	-4.7793	1.8784
10	-4.1709	1.6293	30	-4.0058	1.3853
15	-3.8074	1.3488	45	-2.9180	1.0427
20	-3.5492	1.1508	60	-2.2292	0.8629
25	-2.9969	0.9912	75	-1.5284	0.6839
35	-2.3952	0.7290	90	-1.2615	0.5731
40	-2.2435	0.6584	105	-0.7931	0.4578
45	-1.9421	0.5270	120	-0.7043	0.3693
50	-1.8396	0.5211			
55	-1.7547	0.4439			
65	-1.5247	0.3434			
75	-1.3306	0.2569			

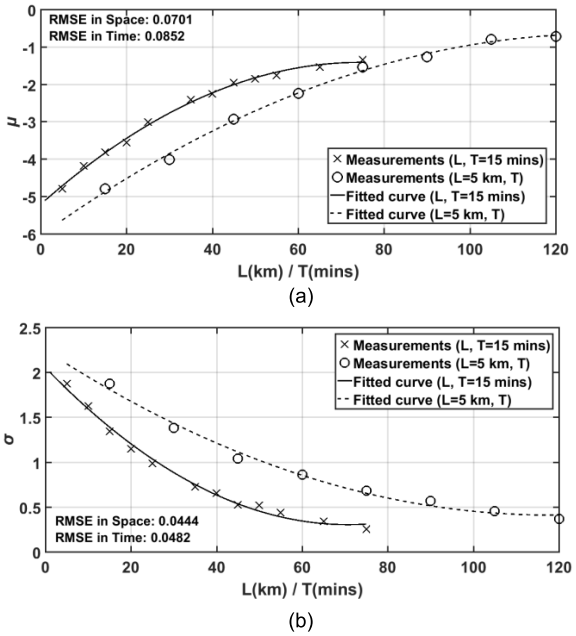

FIGURE 3. Plot of lognormal distribution parameters μ for different space scales when $T = 15mins$ and different time scales when $L = 5km$ (for Portsmouth UK): (a) plot of μ, and (b) plot of σ.

TABLE 5. Fitted coefficient values of Eq. (12) for lognormal parameters in both space and time domains.

	μ			σ		
	p_1	p_2	p_3	p_1	p_2	p_3
Space	−0.007	0.1037	−5.2292	0.0003	-0.0493	2.0536
Time	-0.003	0.0810	-5.9859	0.0001	-0.0314	2.2591

order polynomial:

$$\psi(x) \approx \sum_{k=0}^{2} p_k x^{2-k} \tag{12}$$

which is appropriate to conveniently downscaled $\{\mu, \sigma\}$ to any other space-time scales with reasonable accuracy. In this particular example the polynomial coefficients are given in Table 5. This polynomial conversion has been used extensively to downscale $\{\mu, \sigma\}$ values to other scales of interest and validated using rain rate distribution estimates.

From the ITU-R P.838-7 [45], rain rate exceedance distribution is required by radio communications engineers, and the percentage of exceeded rain rate between $R_{0.001}$ and $R_{0.01}$

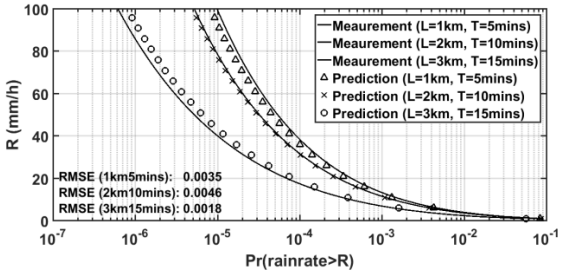

FIGURE 4. Complementary cumulative distribution function of rainfall rate for different spatial-temporal integration lengths.

is of particular important. The study in [41] showed that the first and second order moments of rainfall rates are:

$$E\{R\} = P_0 \exp\left(\mu + \frac{\sigma^2}{2}\right) \equiv \mu_R \tag{13}$$

and

$$E\{R\}^2 = P_0 \exp\left(2\mu + \sigma^2\right), \tag{14}$$

and the variance of R is:

$$\sigma_R^2 = P_0\left[\exp\left(\sigma^2\right) - 1\right]\exp\left(2\mu + \sigma^2\right). \tag{15}$$

Therefore the lognormal parameters at other space-time scales can be derived as follows:

$$\mu\,(L,T) = ln\left(\frac{\mu_R}{P_0\,(L,T)}\right) - \frac{1}{2} - \frac{P_0\,(L,T)\,\sigma_R^2\,(L,T)}{\mu_R} \tag{16}$$

$$\sigma\,(L,T) = \sqrt{1 + \frac{P_0\,(L,T)\,\sigma_R^2\,(L,T)}{\mu_R}} \tag{17}$$

The exceeded rain distribution can be plotted using

$$P_{\mathcal{R}}\{R > \mathcal{R} | \mathcal{R} > 0\} = P_0\,(L,T) \times Q\left(\frac{lnR - \mu\,(L,T)}{\sigma\,(L,T)}\right) \tag{18}$$

where Q() is the complementary error function, $\mathcal{R}$ is the given rain rate and $P_{\mathcal{R}}$ represents the percentage of exceedance of that given rain rate.

Fig. 4 compares the rainfall rate exceedance distributions for Portsmouth at different combinations of space-time scales using model-derived $\{P_0, \mu, \sigma\}$ and the calculated values from measured radar data. The results of three combinations ($\{1\,km, 5mins\}$, $\{2\,km, 10\,mins\}$ and $\{3\,km, 15\,mins\}$) are presented. Fig. 4 show that the exceeded rainfall rate distributions yielded by the model and calculated from radar measured data are accurate with root mean square errors of less than 0.005. The rainfall rate exceeded for 0.01% of time is approximately between 18 mm/h and 37 mm/h depending on the spatial-temporal integration length. In addition, $R_{0.01}$ value from ITU-R P838-7 is about 45 mm/h for Portsmouth, which is higher than the model prediction and values calculated from measured data. This is consistent with the findings in many other studies. For example, in [46] the authors evaluated 1-mins rain rate interpolation models and compared

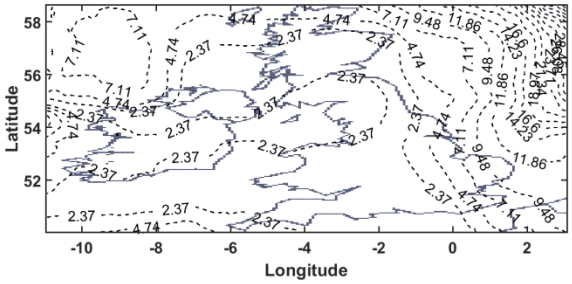

FIGURE 5. Contour maps of error percentage of $R_{0.01}$ over the British Isle at spatial integration length of 1*km* and temporal period of 5*mins*.

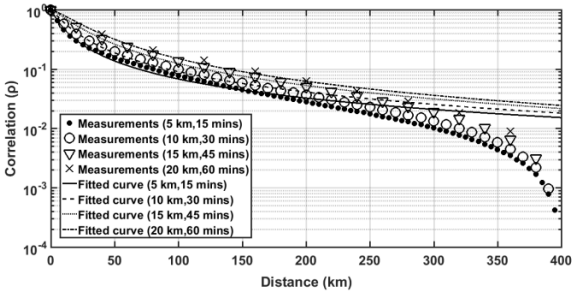

FIGURE 6. Space correlation functions of rainfall rate at different space-time scales (Portsmouth).

the results of $R_{0.01}$ exceedance distribution with ITU-R model for nine sites in South Korea. They obtained error percentage of 3.32% and 12.59% for 5-mins and 10 mins conversions, respectively, to 1 min but the error percentage increases rapidly for conversions from longer duration measurements. The ITU-R P838-7 model is a general model and therefore is not accurate at specific locations. Hence the ITU recommends that users should use their own data to produce better results. Assessments show that the model proposed in this paper provides good estimates of P_0 at the scale range between $\{100\,m, 20\,s\}$ and $\{35\,km, 60\,mins\}$. However an assessment of accuracy for all space-time scales could not be ascertain due to lack of data at all space-time resolutions.

To reduce computation time, the authors have created databases for users to easily obtain the rain characteristic parameter values using Eq. (19) and (20) [33] to convert the coordinates into longitude and latitude values at location of interest;

$$z_{(longitude)} = 0.0658y - 19.8364 \tag{19}$$

$$z_{(latitude)} = -0.0409y + 59.430 \tag{20}$$

where y denotes either row or column number of the NIMROD data grid and z is the corresponding coordinate value in either latitude or longitude.

$R_{0.01}$ has been analyzed over the whole of the British Isles using the downscaled data from the proposed model and the error percentages (E) between the model estimates and values calculated from UK measured data is calculated using

$$E = \frac{|P_v - M_v|}{M_v} \times 100\% \tag{21}$$

where, P_v and M_v are the model predicted and measured values, respectively.

An example of a contour map of error percentage of $R_{0.01}$ at scale of $\{L = 1\,km, T = 5\,mins\}$ is presented for discussion. Fig. 5 shows that the model accuracy for the British Isles is very high with error percentage values generally lower than 2.5% except in the south-east of England. However, the E value tends to be high towards the edges of radar scan region due to insufficient data, especially in the oceanic area.

C. CORRELATION FUNCTION OF RAIN

High frequency wireless networks planning require knowledge of the horizontal structure of rain fields and the evolution of rain events. The analysis of the correlation properties of rain is not always straightforward due to non-stationary, non-homogeneous and irregular rainfall patterns. To simplify the study, the spatial structure of rainfall field is usually assumed to be homogeneous and isotropic such that the space correlation function only depends on the separation distance $d = |\mathbf{x} - \mathbf{y}|$. Given that such assumptions are only valid over small areas and short time periods, they allow the effects caused by factors such as rainfall field shape as well as intermittent sampling of rain events to be avoided.

The general empirical equation for both the space and time correlation, $C_R^{exp}(f)$, of rainfall rate obtained from NIMROD rain radar maps takes the form [34]:

$$C_R^{exp}(f) = \frac{a}{a + f^n} \tag{22}$$

where $a > 0$ and $n > 0$ are parameters to be determined from data and f can either be d (where d represents the distance in kilometer) or t (where t is the time lag in minutes).

$C_R^{exp}(d)$ was analyzed at a range of combinations of spatial-temporal integration lengths. Fig. 6 shows a plot of the correlation coefficient values as a function of the separation distance for four randomly chosen space-time scales at Portsmouth. The curves are the best fit curves using Eq. (22). The root mean square errors (RMSE) between the correlation coefficients derived from measured data and those calculated using estimates of a and $n$for a number of space-time combinations are presented in Table 6. It shows that Eq. (22) gives accurate estimates of the correlation coefficient values for a wide range of integration scales. Longer integration lengths yield higher values than smaller ones due to the averaging out of local variations that exist at smaller dimensions. The near linear sections in Fig. 6 suggest an exponential tendency of the correlation coefficient with distance, and this is true for other combinations of space-time integration volumes although the results are not presented in this paper. It also indicates that the exponential law is appropriate for the prediction of rainfall field structure for North West Europe.

Correlation coefficient of rainfall in time, $C_R^{exp}(t)$, is also an important parameter for the design and implementation of fade mitigation techniques, especially for links with high elevation paths. Considering rain cloud movement and the evolution of rain events, it can be argued that time correlation of rainfall is primarily affected by advection. The same as in

TABLE 6. Coefficient values of space correlation functions of rainfall rate at selected spatial-temporal integration length at Portsmouth.

Integration length $\{L, T\}$	a_L	n_L	RMSE
$\{5\,km, 15\,mins\}$	12.92	1.12	0.011
$\{10\,km, 30 mins\}$	27.93	1.22	0.023
$\{15\,km, 45\,mins\}$	45.92	1.31	0.037
$\{20\,km, 60\,mins\}$	58.99	1.34	0.065

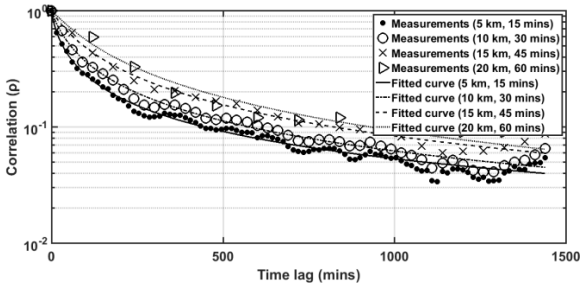

FIGURE 7. Time correlation functions of rainfall rate at different space-time scales (Portsmouth).

TABLE 7. Coefficient values of temporal correlation functions of rainfall rate for different spatial-temporal integration lengths at Portsmouth.

Integration length $\{L, T\}$	a_T	n_T	RMSE
$\{5\,km, 15\,mins\}$	18.75	0.84	0.007
$\{10\,km, 30 mins\}$	44.03	0.94	0.036
$\{15\,km, 45\,mins\}$	58.24	0.98	0.073
$\{20\,km, 60\,mins\}$	72.68	1.01	0.156

space, $C_R^{exp}(t)$ at different integrated space-time scales was studied. Fig. 7 shows plots of the calculated and fitted correlation coefficients as a function of time. The time correlation of rainfall also significantly changes with varying spatial-temporal integration lengths. The longer the integration time, the smoother the time correlation would be due to decreasing variance with increasing integration period. However, the correlation coefficient values become unpredictable when the time lag is longer than 1000*mins* and the space resolution exceeds 30*km* for time resolution of 120*mins*at one location. It also shows that the fitted curves using Eq. (22) agree well with the measured data with RMSE ranging from 0.007 for $\{5\,km, 15\,mins\}$ to 0.156 for $\{20\,km, 60\,mins\}$. The best fit coefficient values for $C_R^{exp}(t)$ with increasing space-time scales are given in Table 7.

From Table 6 and 7, it is noted that the coefficients $\{a, n\}$in both space and time domains increase with increasing integration volumes, and this has been confirmed after analysis of the integrated data with a wide range of combinations of space-time scales between $\{5\,km, 15\,mins\}$ and $\{20\,km, 60\,mins\}$.

Eq. (22) therefore can be written in the form

$$C_R^{exp}(f) \cong \frac{a_\psi(L,T)}{a_\psi(L,T) + f^{n_\psi(L,T)}} \tag{23}$$

with factorable parameters, for a set of values of distance d or time t. The coefficients $a_\psi(L,T)$ and $n_\psi(L,T)$ explicitly

TABLE 8. Parameter values of Eq. (24) and Eq. (25) at Portsmouth.

parameter	Space correlation	Time correlation
b_1	1.6231	1.9714
b_2	1.0010	1.0200
b_3	0.6192	0.7033
b_4	0.8394	0.8810
b_5	0.9010	0.9311
c_1	10	10
c_2	−11.3352	−11.6513
c_3	−0.0846	−0.0893
c_4	0.0513	0.0289
c_5	−0.1291	−0.1216
c_6	0.0686	0.0701

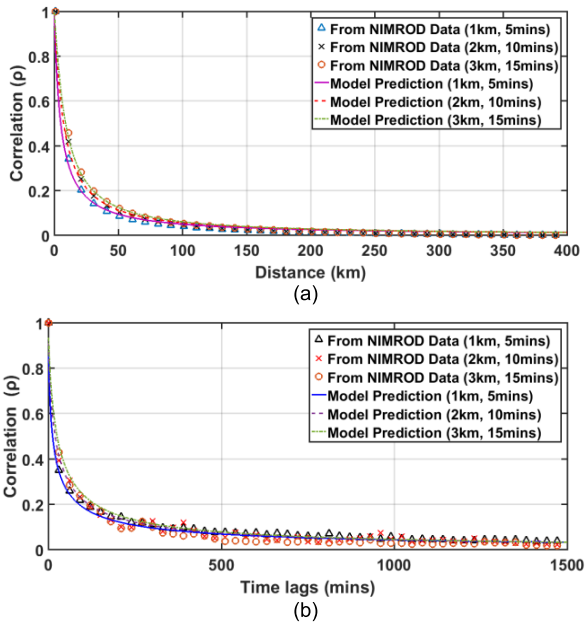

FIGURE 8. Comparison of measured and model predicted correlation function of rainfall rate at Portsmouth, (a) is space correlation, and (b) is time correlation.

depend on the space resolution, L, and time interval, T. Models that have been derived and proposed in this paper to represent these coefficients for all locations at varying space-time combinations can be expressed as:

$$a_\psi(L,T) \cong b_1 L^{b_2} + b_3 T^{b_4} + b_5 \tag{24}$$

$$n_\psi(L,T) \cong c_1 + c_2 e^{(c_3 L^{c_4} + c_5 T^{c_6})} \tag{25}$$

where $b_1, \ldots b_5$, and $c_1, \ldots c_6$ can be determined using non-linear least square method.

The specific forms of Eq. (24) and Eq. (25) are developed primarily to allow efficient computation without significant loss of accuracy. However, an assurance of accuracy is based on sacrificing algebraic tractability as a result of the numerous coefficients involved.

Given that UK NIMROD holds another database for the British Isles with the higher resolutions of $1\,km$ in space and $5\,mins$ in time, the correlation coefficient values at a number of space-time combinations that are smaller than $\{5\,km, 15\,mins\}$ have been calculated from the data. The values of the coefficients in Eq. (24) and Eq. (25) for Portsmouth

are presented as an example, the fitted coefficient values are given in Table 8.

A comparison of the correlation coefficient values of rainfall rate calculated from measured data and the proposed model prediction are presented in Fig. 8. The model predictions show high agreement with real measurements at different space-time scales for both space and time correlation with averaged RMSE of 0.025 in space and 0.049 in time. This is true for other combinations. This shows that Eq. (24) and Eq. (25) can be applied to estimate rain characteristic parameters at space and time resolutions for which there is no data, particularly at higher resolutions. The application of the proposed model also serves to reduce the long computing time often required to process data to obtain correlation coefficient values of rain at multiple space-time scales.

V. CONCLUSION

This paper has proposed a numerical models that can be used to predict point rainfall rate in space and time simultaneously, particularly at higher resolutions than are currently available from NIMROD rain radar. Dynamic description of the parameters associated with rain field estimates has been presented with extensive investigation of area-time average of rainfall rate. This is because integration over varying spatial and temporal integration lengths changes the first and second order statistics of rainfall rate and thus rain-induced attenuation on radio links.

The paper has proposed a set of empirical equations that can be used to estimate rain parameters at varying space-time scales with fairly high accuracy. The results have been validated by comparing model predictions with values calculated from measured data. Databases of rain parameters spanning North West Europe have been produced for users to conveniently obtain rain rate information at any location of interest for any combination of spatial-temporal integration lengths. This offers great convenience as almost no computation time is required. Given these databases, the prediction of rain characteristics at other space-time resolutions, especially those that are not available from rain radar measurements, can be obtained. The accuracy was tested by analyzing the rain rate exceedance distribution at different space-time scales and the model validity is for space and time scales between $\{100\,m, 20\,s\}$ and $\{35\,km, 60\,mins\}$.

A contour map of the error percentage (E) of exceeded rain rate value of $R_{0.01}$ for the British Isle at the scale of $\{L = 1\,km, T = 5\,mins\}$ has been presented and the results show that the error percentage is very low for the continental area where the calculated E is less than 3% for all areas apart from the south-east of England. It has also been noted that the E values tend to be high towards the edges of radar scan region, such as the oceanic area due to low availability or lack of data. An empirical model to estimate the correlation coefficient values at any location for a wide range of time and space separation and validated using measured data. The model estimates the correlation coefficient with RMSE of less than 0.03 in space and 0.05 in time. The model will not only help researchers and practitioners estimate values at time and space separations at which they may not have data but reduce the time it takes to compute the values from measured data.

The models proposed in this paper will assist engineers and scientists in developing a number applications, e.g. allocating additional satellite resources to mitigate against adverse weather conditions, site diversity techniques and instantaneous joint fade experienced by all links in a microwave network, etc.. It is particularly true for satellite network systems where the optimization of an adaptive onboard common resource-sharing system and fade mitigation technique require detailed knowledge of the space-time characterization of rain fields. The models proposed in this paper can be applied to a detailed study of rain attenuation statistics at any location in North West Europe.

ACKNOWLEDGMENT

The authors wish to thank the British Atmospheric Data Centre (BADC), which is part of the Centre for Environmental Data Analysis (CEDA), and the British Met Office for providing access to the NIMROD rain radar data.

REFERENCES

[1] R. K. Crane, *Electromagnetic Wave Propagation Through Rain*. Hoboken, NJ, USA: Wiley, 1996.

[2] A. D. Panagopoulos and J. D. Kanellopoulos, "On the rain attenuation dynamics: Spatial-temporal analysis of rainfall rate and fade duration statistics," *Int. J. Satell. Commun. Netw.*, vol. 21, no. 6, pp. 595–611, Nov. 2003.

[3] B. C. Gremont and M. Filip, "Spatio-temporal rain attenuation model for application to fade mitigation techniques," *IEEE Trans. Antennas Propag.*, vol. 52, no. 5, pp. 1245–1256, May 2004.

[4] S. Shrestha and D.-Y. Choi, "Study of 1-min rain rate integration statistic in South Korea," *J. Atmos. Solar-Terrestrial Phys.*, vol. 155, pp. 1–11, Mar. 2017.

[5] P. K. Kundu and R. K. Siddani, "Scale dependence of spatiotemporal intermittence of rain," *Water Resour. Res.*, vol. 47, no. 8, pp. 1–17, Aug. 2011.

[6] *Rec. 618: Propagation Data and Prediction Methods Required for the Design of Earth-Space Telecommunication Systems*, document Rec. ITU-R, 2015, pp. 612–618.

[7] D. A. Hughes, "Comparison of satellite rainfall data with observations from gauging station networks," *J. Hydrol.*, vol. 327, nos. 3–4, pp. 399–410, Aug. 2006.

[8] M. Valeria, R. Fabio, N. Francesco, L. Federico, and B. Luca, "Study on the rainfall dependence structure using radar and rain gauge data," in *Proc. Int. Workshop Adv. Stat. Hydrol.*, Taomina, Italy, May 2010, p. 16.

[9] D. S. Wilks and R. L. Wilby, "The weather generation game: A review of stochastic weather models," *Prog. Phys. Geography*, vol. 23, no. 3, pp. 329–357, Sep. 1999.

[10] C. Onof, R. E. Chandler, A. Kakou, P. Northrop, H. S. Wheater, and V. Isham, "Rainfall modelling using Poisson-cluster processes: A review of developments," *Stochastic Environ. Res. Risk Assessment*, vol. 14, no. 6, pp. 0384–0411, Nov. 2000.

[11] K. S. Paulson, C. Ranatunga, and T. Bellerby, "A method to estimate trends in distributions of 1 min rain rates from numerical weather prediction data," *Radio Sci.*, vol. 50, no. 9, pp. 931–940, Sep. 2015.

[12] R. Deidda, "Rainfall downscaling in a space-time multifractal framework," *Water Resour. Res.*, vol. 36, no. 7, pp. 1779–1794, Jul. 2000.

[13] P. K. Kundu and R. K. Siddani, "Scale dependence of spatiotemporal intermittence of rain," *Water Resour. Res.*, vol. 47, no. 8, Aug. 2011. W08522

[14] A. Pathirana, S. Herath, and T. Yamada, "Estimating rainfall distributions at high temporal resolutions using a multifractal model," *Hydrol. Earth Syst. Sci.*, vol. 7, no. 5, pp. 668–679, 2003.

[15] D. Veneziano, R. L. Bras, and J. D. Niemann, "Nonlinearity and self-similarity of rainfall in time and a stochastic model," *J. Geophys. Res., Atmos.*, vol. 101, no. D21, pp. 26371–26392, Nov. 1996.

[16] X. Yang, X. Xie, D. L. Liu, F. Ji, and L. Wang, "Spatial interpolation of daily rainfall data for local climate impact assessment over greater sydney region," *Adv. Meteorol.*, vol. 2015, pp. 1–12, Jun. 2015.
[17] H. Basarudin, H. F. Rozi, A. F. Ramli, and M. I. Sulaiman, "Initial study of applying random midpoint displacement for rain Radar's rain rate interpolation," in *Proc. Int. Conf. Eng. Technol. Technopreneurship (ICE2T)*, Kuala Lumpur, Malaysia, Sep. 2017, pp. 18–20.
[18] A. Foehn, J. García Hernández, B. Schaefli, and G. De Cesare, "Spatial interpolation of precipitation from multiple rain gauge networks and weather radar data for operational applications in alpine catchments," *J. Hydrol.*, vol. 563, pp. 1092–1110, Aug. 2018.
[19] X. Yang, X. Xie, D. L. Liu, F. Ji, and L. Wang, "Spatial interpolation of daily rainfall data for local climate impact assessment over greater sydney region," *Adv. Meteorol.*, vol. 2015, pp. 1–12, Jul. 2015, doi: 10.1155/2015/563629.
[20] K. S. Paulson and X. Zhang, "Simulation of rain fade on arbitrary microwave link networks by the downscaling and interpolation of rain radar data," *Radio Sci.*, vol. 44, no. 2, pp. 1–10, Apr. 2009.
[21] K. S. Paulson, "Fractal interpolation of rain rate time series," *J. Geophys. Res., Atmos.* vol. 109, no. D22, pp. 1–8, Nov. 2004.
[22] B. Gremont, M. Filip, P. Gallois, and S. Bate, "Comparative analysis and performance of two predictive fade detection schemes for ka-band fade countermeasures," *IEEE J. Sel. Areas Commun.*, vol. 17, no. 2, pp. 180–192, Feb. 1999.
[23] R. Nebuloni, C. Capsoni, M. Luccini, and L. Luini, "Assessment of rain fade mitigation techniques for high throughput satellites by a time series synthesizer," in *Proc. 9th Eur. Conf. Antennas Propag.*, Apr. 2015, pp. 13–17.
[24] S. Perica and E. Foufoula-Georgiou, "Model for multiscale disaggregation of spatial rainfall based on coupling meteorological and scaling descriptions," *J. Geophys. Res., Atmos.*, vol. 101, no. D21, pp. 26347–26361, Nov. 1996.
[25] V. Venugopal, E. Foufoula-Georgiou, and V. Sapozhnikov, "A space-time downscaling model for rainfall," *J. Geophys. Res., Atmos.*, vol. 104, no. D16, pp. 19705–19721, Aug. 1999.
[26] R. Deidda, M. G. Badas, and E. Piga, "Space–time multifractality of remotely sensed rainfall fields," *J. Hydrol.*, vol. 322, nos. 1–4, pp. 2–13, May 2006.
[27] G. I. Taylor, "The spectrum of turbulence," in *Proc. Roy. Soc. London A, Math., Phys. Eng. Sci.*, vol. 164, no. 919, Feb. 1938, pp. 476–490.
[28] G. Yang, B. Gremont, D. Ndzi, and D. J. Brown, "Characterization of rain fields for UK satellite networks," in *Proc. Ka Broadband Commun., Navigat. Earth Observ. Conf.*, Oct. 2011, pp. 1–7.
[29] L. Luini and C. Capsoni, "The impact of space and time averaging on the spatial correlation of rainfall," *Radio Sci.*, vol. 47, no. 3, pp. 1–10, Jun. 2012.
[30] B. Kedem and L. S. Chiu, "On the log-normality of rain rate," *Proc. Nat. Acad. Sci. USA*, vol. 84, no. 4, pp. 901–905, 1987.
[31] P. V. Mandapaka, W. F. Krajewski, G. J. Ciach, G. Villarini, and J. A. Smith, "Estimation of radar-rainfall error spatial correlation," *Adv. Water Resour.*, vol. 32, no. 7, pp. 1020–1030, Jul. 2009.
[32] T. L. Bell, "A space-time stochastic model of rainfall for satellite remote-sensing studies," *J. Geophys. Res.*, vol. 92, no. D8, p. 9631, Aug. 1987.
[33] G. Yang, D. Ndzi, K. Paulson, M. Filip, and A.-H. Al-Hassani, "Rainfall Rate Field Space-Time Interpolation Technique for North West Europe," *Prog. Electromagn. Res. M*, vol. 83, pp. 93–107, 2019.
[34] G. Yang, D. L. Ndzi, B. C. Gremont, K. Paulson, M. Filip, and A.-H. Al-Hassani, "The impact of spatial–temporal averaging on the dynamic–statistical properties of rain fields," *IEEE Trans. Antennas Propag.*, vol. 67, no. 12, pp. 7505–7517, Dec. 2019, doi: 10.1109/TAP.2019.2930137.
[35] R. J. Doviak and D. S. Zrnic, *Doppler Radar and Weather Observations*, 2nd ed. New York, NY, USA: Academic, 1993, p. 592.
[36] D. L. Harrison, S. J. Driscoll, and M. Kitchen, "Improving precipitation estimates from weather radar using quality control and correction techniques," *Meteorlogical Appl.*, vol. 7, no. 2, pp. 135–144, Jun. 2000.
[37] B. W. Golding, "Nimrod: A system for generating automated very short range forecasts," *Meteorological Appl.*, vol. 5, no. 01, 1998, pp. 1–16. [Online]. Available: http://badc.nerc.ac.uk/browse/badc/uk-nimrod/doc/
[38] *National Meteorological Library and Archive Fact Sheet 15—Weather Radar*, Met Office, Exeter, U.K., 2009.
[39] E. Matricciani, "Physical-mathematical model of the dynamics of rain attenuation based on rain rate time series and a two-layer vertical structure of precipitation," *Radio Sci.*, vol. 31, no. 2, pp. 281–295, Mar. 1996.
[40] *Specific Attenuation Model for Rain For Use in Prediction Methods*, document Rec. ITU-R P. 838-3, Geneva, Switzerland, 2005.
[41] G. Yang, B. Christian Gremont, L. Yang, M. E. Ibrahim, and L. Bai, "Space–time channel model for rain-affected communication networks," *IEEE Trans. Antennas Propag.*, vol. 67, no. 7, pp. 4768–4776, Jul. 2019, doi: 10.1109/TAP.2019.2907601.
[42] A. Papoulis and S. U. Pillai, "*Probability, Random Variables and Stochastic Processes*, 4th ed. New York, NY, USA: McGraw-Hill, 2002.
[43] M. Filip and E. Vilar, "Optimum utilization of the channel capacity of a satellite link in the presence of amplitude scintillations and rain attenuation," *IEEE Trans. Commun.*, vol. 38, no. 11, pp. 1958–1965, Nov. 1990.
[44] G. Yang, "Rainfall rate modelling for European satellite networks," Ph.D. dissertation, Univ. Portsmouth, Portsmouth, U.K., 2016.
[45] *Characteristics of Precipitation for Propagation Modelling*, document ITU-R Rec., Geneva, Switzerland, 2017, pp. 7–837.
[46] S. Shrestha, J.-J. Park, and D.-Y. Choi, "Rain rate modeling of 1-min from various integration times in South Korea," *SpringerPlus*, vol. 5, no. 1, p. 433, Dec. 2016.